J Mater Sci (2007) 42:9730–9735
DOI 10.1007/s10853-007-1995-x

Structure and crystallization behavior of borate-based bioactive glass

Aihua Yao · Mohamed N. Rahaman · Jian Lin · Wenhai Huang

Received: 22 April 2007 / Accepted: 13 July 2007 / Published online: 20 August 2007

Abstract The structure and crystallization behavior of borate-based bioactive glass, designated 45S5B1, were investigated by Fourier transform infrared (FTIR) spectroscopy, differential thermal analysis (DTA), X-ray diffraction (XRD), and scanning electron microscopy (SEM). FTIR spectroscopy revealed that the network structure of the glass consisted mainly of $[BO_3]$, $[BO_4]$ and $[PO_4]$ units. Two distinct crystallization peaks were observed for this glass by DTA, with activation energies of 475 and 210 kJ/mol, respectively. XRD indicated that the crystallization process with higher activation was associated with the formation of $CaNa_3B_5O_{10}$, whereas the process with the lower activation energy was associated with the formation of CaB_2O_4. The results indicated that the crystallization process in 45S5B1 glass was dominated by bulk crystallization, although surface crystallization also occurred for small particle sizes (<50 μm).

Introduction

Since the initial report on its bone-bonding property by Hench et al. [1], silicate-based bioactive glass, designated 45S5, with a typical composition (in mol%) of 24.4 Na_2O, 26.9 CaO, 2.6 P_2O_5, 46.1 SiO_2, has been intensively investigated for biomedical applications. Whereas 45S5 glass has excellent bioactive characteristics, it is only partially converted to hydroxyapatite (HA), the main mineral constituent of bone, when immersed in physiological media. For 45S5 glass particles of size 150–300 μm, less than 50% (by weight) was converted to HA in an aqueous phosphate solution after several weeks, when the conversion effectively stopped, leaving a core of unconverted glass [2].

Borate glass, based on B_2O_3 network as opposed to the SiO_2 network for silicate glasses, may provide an alternative bioactive glass to 45S5 for biomedical applications such as bone repair. A borate glass, designated 45S5B1, with the same molar composition as 45S5 glass but with all the SiO_2 replaced by B_2O_3, has been shown to undergo more rapid and complete conversion to HA in a dilute aqueous phosphate solution [2, 3]. Particles (150–300 μm) of 45S5B1 glass were almost completely converted to HA in less than 4 days when immersed in a 0.02 M K_2HPO_4 solution with a starting pH value of 7.0 at 37 °C [2].

Bioactive glass-ceramics have been the subject of numerous investigations in the last few years because they can provide improved mechanical properties when compared to the parent glass. The crystallization and sintering of bioactive glasses may significantly influence their bioactivity and cellular reactions, as well as their mechanical properties [4–6]. However, the reports on the crystallization kinetics of bioactive glasses are limited [4]. The objective of the present work was to investigate the crystallization behavior of borate-based 45S5B1 bioactive glass. Differential thermal analysis (DTA) at different heating rates was used to determine the activation energy and crystallization behavior, whereas X-ray diffraction (XRD) and scanning electron microscopy (SEM) were used to investigate the structural characteristics of the crystallization. An understanding of the crystallization behavior

A. Yao (✉) · J. Lin · W. Huang
School of Materials Science and Engineering, Tongji University, 1239 Siping Road, Shanghai 200092, P.R. China
e-mail: aihyao@126.com

A. Yao · M. N. Rahaman
Department of Materials Science and Engineering, University of Missouri, Rolla, MO 65409, USA

of 45S5B1 glass may be useful for controlling its bioactive potential, degradation behavior, and mechanical properties, which is important for biomedical applications such as bone repair.

Theoretical analysis of crystallization behavior

DTA has been extensively employed to investigate the thermal behavior and crystallization kinetics of glass under non-isothermal conditions [7–10]. Several analytical models are available to determine the kinetic parameters associated with glass crystallization, but the Kissinger model is the most widely used. According to the Kissinger model, the activation energy for crystallization E_c is given by the equation:

$$\ln\left(\frac{\alpha^n}{T_p^2}\right) = -\frac{E_c}{RT_p} + C \quad (1)$$

where α is the heating rate, n is a constant known as the Avrami exponent, R is the gas constant, T_p is the exothermic peak temperature and C is a constant. A plot of $\ln\left(\alpha^n / T_p^2\right)$ versus $1/T_p$ gives a straight line with a slope of $-E_c/R$, from which E_c is obtained.

The Avrami exponent n can be determined by Ozawa's equation [11]:

$$\frac{d\ln[-\ln(1-x)]}{d\ln\alpha}\Big|_T = -n \quad (2)$$

where x is the volume fraction crystallized at a temperature T for a constant heating rate α. As shown in Fig. 1, $x = A_i/A$, where A is the area under DTA curve between T_1, the temperature at which crystallization starts, and T_2, the temperature at which crystallization is completed, and A_i is the area under the curve between T_1 and T. The crystallization of a glass can occur either from the surface or uniformly in the bulk. A value of n close to 3 signifies bulk or three-dimensional crystallization and a value close to 1 indicates surface crystallization. Intermediate values of n between 1 and 3 are indicative of a combination of surface and bulk crystallization [12, 13].

Experimental

Borate-based bioactive glass, designated 45S5B1, with the composition (in mol%): 24.4 Na_2O, 26.9 CaO, 2.6 P_2O_5, 46.1 B_2O_3, was prepared by melting the required quantities of reagent grade Na_2CO_3, $CaCO_3$, H_3BO_4 and NaH_2PO_4 $2H_2O$ in a Pt crucible in air for 1 h at 1,100 °C. The melt was quenched by pouring it on a steel plate and pressed with another plate to obtain glass plates with a thickness of

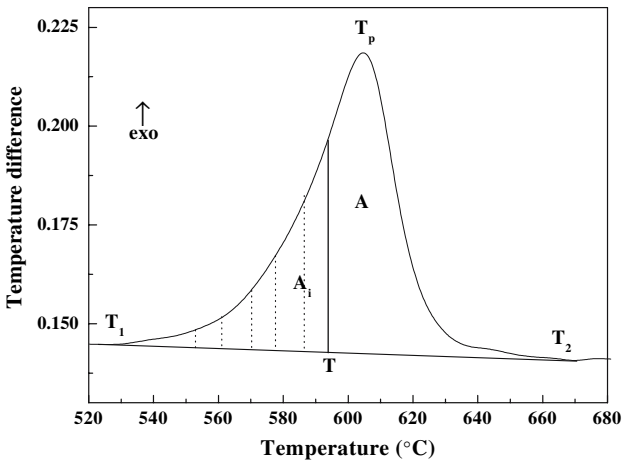

Fig. 1 Illustration of method used for calculating the volume fraction of crystals during non-isothermal DTA

1–1.5 mm. Glass particles of size <50 μm were obtained by crushing the glass in a hardened steel mortar and pestle, followed by classification using stainless steel sieves.

Differential thermal analysis (Model DTA7; Perkin Elmer Corp., Eden Prairie, MN) was performed by heating 40 mg of the glass particles in air in a Pt crucible at constant heating rates of 5, 10, 15 and 20 °C/min. α-Al_2O_3 powder was used as the reference material, and the instrument was calibrated periodically using In, Zn and Ag as standards. Phases present in the heat-treated glass powder were identified using X-ray diffraction, XRD (Scintag XDS2000) using Cu K_α radiation (λ = 0.15406 nm) in a step-scan mode (0.05° per step) in the range 5–60° 2θ. Fourier transform infrared (FTIR) analysis (Model 1760-X; Perkin Elmer) of the as-quenched glass and the heat-treated glass was performed in the wavenumber range of 400–4,000 cm^{-1}, on disks prepared from a mixture of 2 mg of the glass powder and 150 mg of high-purity grade KBr. The spectra were corrected by subtracting the KBr spectrum. The surfaces and polished cross sections of heat-treated glass plates (7 mm × 7 mm × 2 mm) were observed using field emission scanning electron microscopy, FE-SEM (Hitachi S-4700). The cross sections were polished with 600 and 1,200 grit of silicon carbide prior to SEM investigation.

Results and discussion

The FTIR spectra of two glass powders prepared from (a) the as-quenched glass and (b) the glass heated at 700 °C, are shown in Fig. 2. The as-quenched glass exhibited broad and smooth bands, whereas the heat-treated glass had sharper bands and more splitting of some bands, which can be attributed to the influence of the crystal field. The

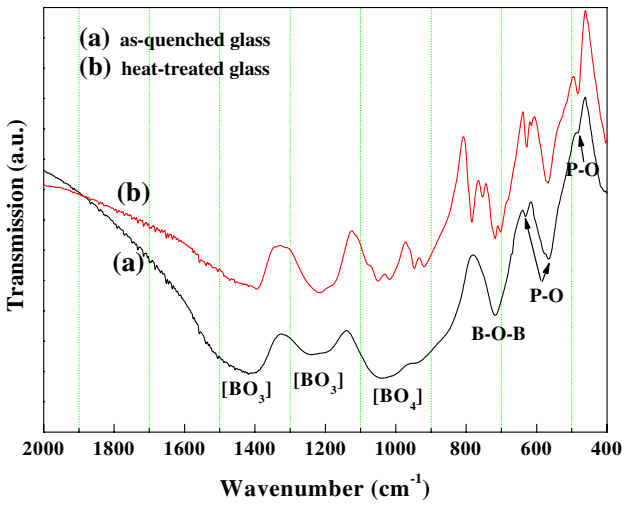

Fig. 2 FTIR spectra of (**a**) particles of as-quenched 45S5B1 glass and (**b**) 45S5B1 glass particles heated at 700 °C

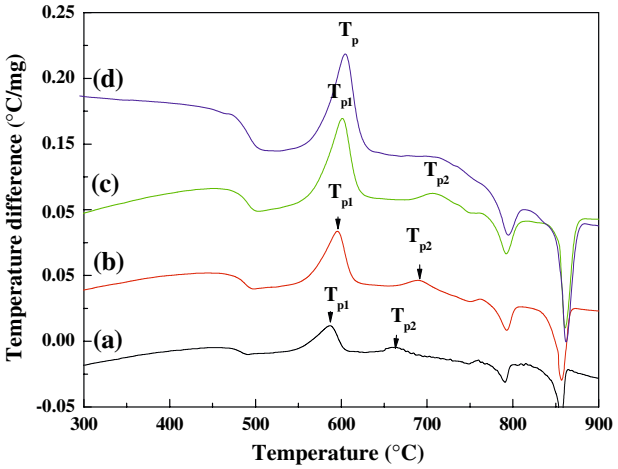

Fig. 3 DTA curves for 45S5B1 glass particles (<50 μm) at heating rates of: (**a**) 5 °C/min, (**b**) 10 °C/min, (**c**) 15 °C/min, (**d**) 20 °C/min

absorption bands in the 1,200–1,500 cm^{-1} and 1150–1300 cm^{-1} ranges were due to B–O stretching of trigonal $[BO_3]$ units, while the absorption bands in the 800–1,200 and 600–800 cm^{-1} ranges were related to B–O stretching of tetrahedral $[BO_4]$ units, and bond-bending motion of B–O–B groups, respectively [14]. A very strong absorption band at 560 cm^{-1} and two weaker ones at around 630 and 480 cm^{-1} were also observed in the FTIR spectra, which originated from the internal modes of PO_4^{3-} ions [15]. Based on these FTIR results, it can be included that $[BO_3]$, $[BO_4]$ and $[PO_4]$ units formed the main structural network in 45S5B1 bioactive glass.

The DTA curves obtained at different heating rates are shown in Fig. 3. The characteristic temperatures, such as glass transition temperature (T_g), onset crystallization temperature (T_x) and crystallization peak temperature (T_p), determined by the software in the DTA instrument are summarized in Table 1. Two distinct crystallization peaks (T_{p1}, T_{p2}) were observed, implying two distinct phase transformations in this glass system. In general, an increase in heating rate from 5 to 20 °C/min resulted in an increase of the peak temperature and the peak height.

Table 1 The characteristic temperatures for 45S5B1 glass determined from DTA curves

Heating rates α (°C /min)	T_g (°C)	Peak 1		Peak 2	
		T_x (°C)	T_p (°C)	T_x (°C)	T_p (°C)
5	478	558	587	650	665
10		567	596	673	690
15		573	601	686	707
20		576	605	665	712

To determine the crystalline phases formed in the heat-treated glass, 45S5B1 glass powders were heated to different temperatures, 480, 500, 680, and 700 °C (heating rate = 10 °C/min), and held at the isothermal temperature for 3 h. These temperatures were selected at the characteristic points in the DTA curves, shown in Table 1. Figure 4 shows the XRD patterns of the as-quenched glass powder and the heat-treated glass powder. The as-quenched glass had an XRD pattern typical of an uncrystallized glass. However, crystallization started to occur when the glass powders were heated at higher temperatures. For the glass heated at 480 °C, peaks were detected in the XRD pattern, which were attributed to the phase $CaNa_3B_5O_{10}$

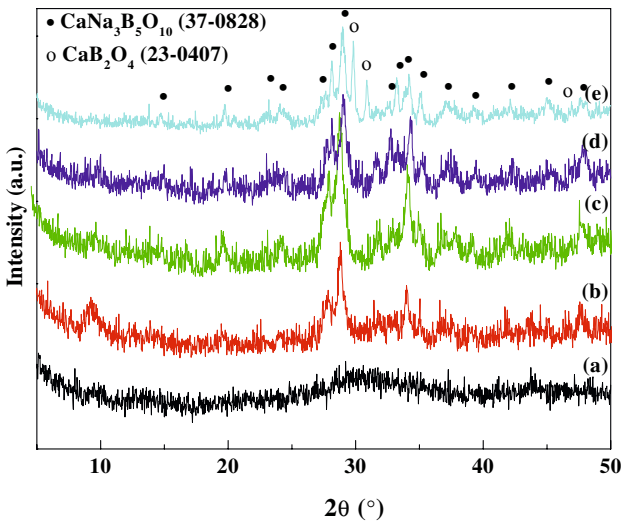

Fig. 4 XRD patterns of as-quenched 45S5B1 glass particles (**a**), and 45S5B1 glass particles heated for 3 h at 480 °C (**b**), 500 °C (**c**), 680 °C (**d**), 700 °C (**e**)

(JCPDS 37-0828). On heating at 680 °C and 700 °C, a crystalline CaB_2O_4 phase was formed (JCPDS 23-0407), in addition to the $CaNa_3B_5O_{10}$ phase.

Figure 5 shows the plots of $\ln[-\ln(1-x)]$ versus $\ln\alpha$ at various temperatures. The Avrami exponent, n, calculated from linear fits to the experimental data using the Eq. 2, was found to be ~ 2, indicating that surface and bulk crystallization proceeded simultaneously in the crystallization process. The occurrence of surface crystallization might be promoted by the small size (<50 μm) and, hence, a large surface area of the glass particles.

Plots of $\ln(\alpha^2 / T_p^2)$ against $1/T_p$ are shown in Fig. 6. The correlation coefficients (R^2) of the plots were all greater than 0.99, indicating good linear relationships. Two distinct activation energies E_{c1} and E_{c2} calculated from the slopes were 475 kJ/mol and 210 kJ/mol, respectively. As found in the FTIR spectra, the main structural units of the 45S5B1 glass network were $[BO_4]$ tetrahedra, $[BO_3]$ triangles and $[PO_4]$. A comparison of the calculated activation energy E_{c1} with the bond strengths of B–O band (476 kJ/mol) [16] and P–O bond (464 kJ/mol) [4] showed that the crystallization of the $CaNa_3B_5O_{10}$ phase was controlled by the breakages of B–O and P–O bands in the glass system, because the value of the activation energy was close to those for the B–O and P–O bond strengths. The crystallization process of CaB_2O_4 phase was believed to be involved the breaking of Ca–O and Na–O bonds, as the respective bond strengths are 111 and 84 kJ/mol [4].

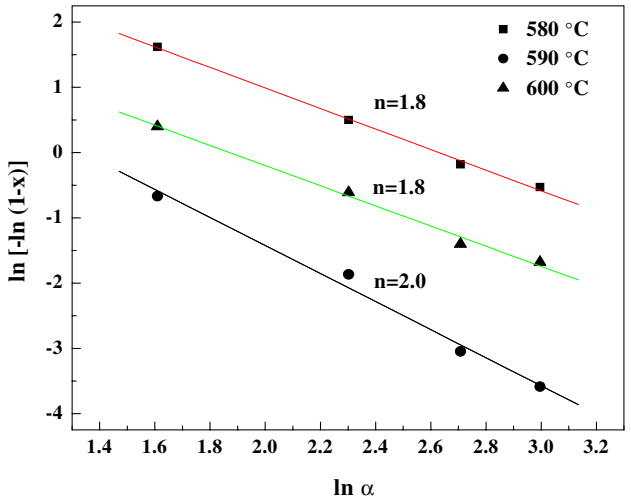

Fig. 5 Plots of $\ln[-\ln(1-x)]$ versus $\ln\alpha$ for 45S5B1 glass particles at 580, 590, 600 °C

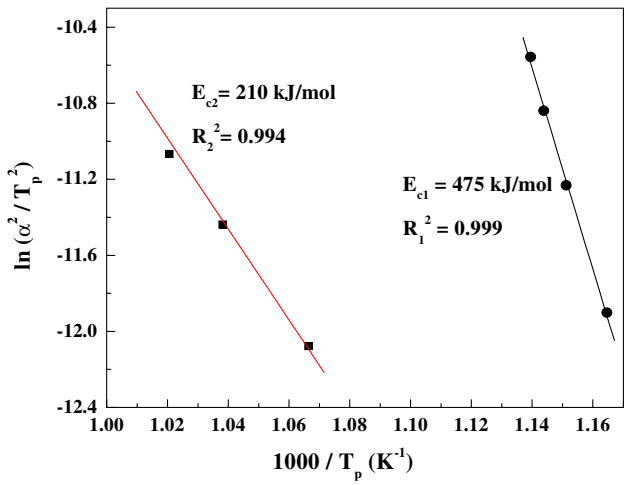

Fig. 6 Kissinger plots of $\ln(\alpha^2/T_p^2)$ against $1/T_p$ for 45S5B1 glass

To further investigate the crystallization mechanism of 45S5B1, a glass plate was heated for 3 h at the nucleation temperature ($\sim$480 °C), and then heated at 10 °C/min to 570 °C to induce crystallization. Figures 7a and b show SEM images of the surface and cross section of the plate after the nucleation step, whereas Fig. 7c shows the cross section of the glass plate after the nucleation and crystallization steps. A large number of crystals were present on the surface of the glass after the nucleation treatment (Fig. 7a), but the bulk appeared to be amorphous, showing no evidence of the presence of crystals (Fig. 7b). According to the XRD results described earlier (Fig. 4), the crystalline phase formed in the glass particles heated at 480 °C was $CaNa_3B_5O_{10}$. In the case of the glass heated to 570 °C, (Fig. 7c), the microstructure consisted of small crystals with a nearly spherical cross section ($\sim$5 μm in diameter) dispersed in a glass matrix. These results indicated that the bulk crystallization was the dominant process for 45S5B1 glass, but surface crystallization also occurred for glass particles with small size [17].

Compared to present borate-based 45S5B1 bioactive glass, silicate-based 45S5 bioactive glass exhibited a different crystallization behavior. According to Clupper and Hench [4], the activation energy for crystallization of 45S5 glass was 350 kJ/mol, and the glass underwent surface crystallization during heat treatment. The difference in the crystallization behavior between 45S5 and 45S5B1 bioactive glass may be due to the difference in bond strengths of the Si–O and B–O bonds of the glass networks. The bond strength of the B–O bond (476 kJ/mol) [16] is higher than that of the Si–O (424 kJ/mol) [4], so a higher energy is required to break B–O band in the process of internal reconstitution and crystallization. Furthermore, Clupper and Hench used a smaller particle size (3 μm avg.), which is expected to promote surface crystallization. In general, a small particle size leads to a crystallization mechanism dominated by surface crystallization, as the surface area is large relative to the total material volume [10].

While borate-based bioactive glass, 45S5B1, undergoes rapid and complete conversion to HA, a concern is the effect of the boron released from the glass on cell [18–20].

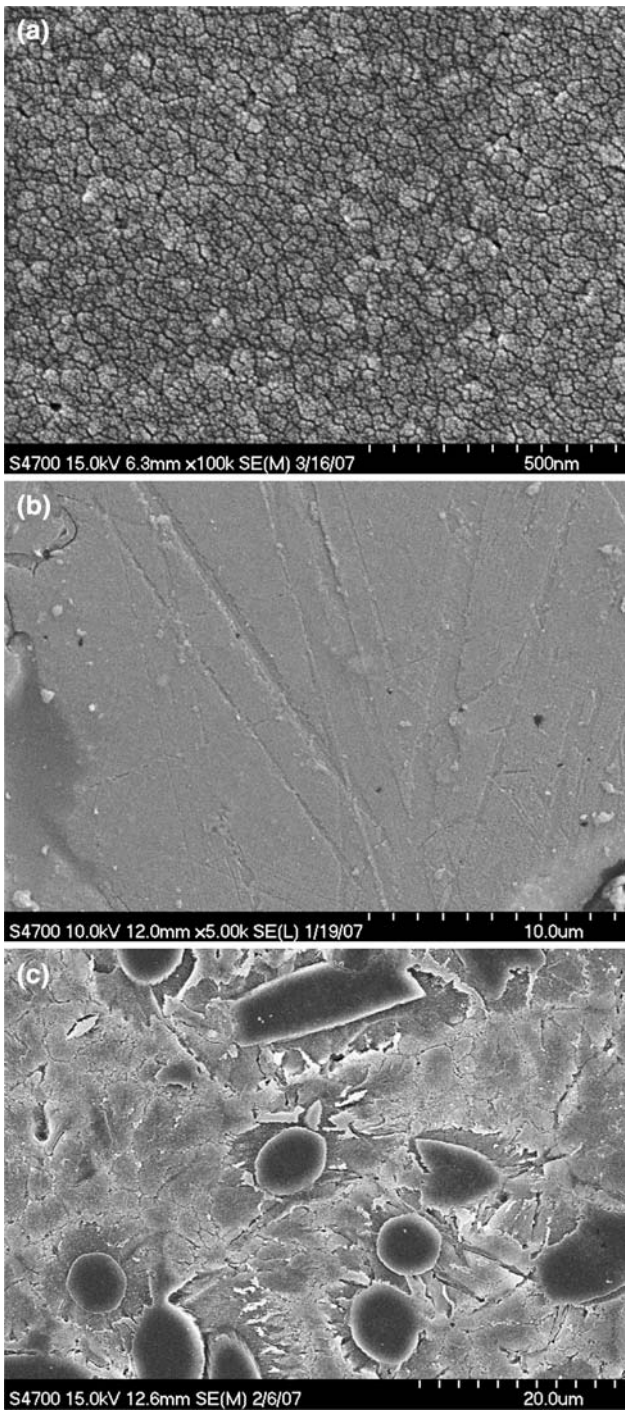

Fig. 7 SEM photographs of (**a**) the surface and (**b**) the cross section of 45S5B1 glass plate nucleated for 3 h at 480 °C; (**c**) the cross section of 45S5 glass plate nucleated for 3 h at 480 °C and heated at 10 °C/min to 570 °C to induce crystallization

It was showed that the concentration of boron ions strongly affected cell attachment and growth. A molarity of 0.002 M boron ions seemed to be the viable limit for cell survival. A concentration of 0.01 M dramatically slowed cell growth, and 0.05 M boron ions eradicated all cellular life within 24 h [20]. Therefore, it is important to control the concentration and rate of boron ions released from the borate-based bioactive glass. A few studies have demonstrated a strong effect of the crystallization on the rate of ion release and exchange, which in turn control the bioactive potential of glass-ceramics [21, 22]. It should therefore be possible to prepare borate-based bioactive glass-ceramics with desirable rates of boron ion release and bioactivity by controlling the nucleation and crystallization of the parent glass. Furthermore, the crystallization is expected to improve the mechanical properties of porous 45S5B1 glass scaffolds for potential load-bearing application, such as bone repair. Currently, the effect of crystallinity on the rate and concentration of boron released from 45S5B1 glass is under investigation.

Conclusion

The crystallization behavior of a borate-based bioactive glass, designated 45S5B1, was investigated using non-isothermal methods by differential thermal analysis. Heat treatment of the glass produced a crystalline phase of predominantly $CaNa_3B_5O_{10}$, but also a small amount of a crystalline CaB_2O_4 phase. Activation energies for the two crystallization processes, determined from the data using the Kissinger equation, were 475 and 210 kJ/mol, respectively. Comparison of these activation energies with the bond strength of the B–O and P–O bonds indicated that the crystallization of the $CaNa_3B_5O_{10}$ phase was controlled by the breaking of B–O bonds, whereas the crystallization process for the CaB_2O_4 phase was more likely associated with the breaking of Ca–O and Na–O bonds. The results of present study indicated that bulk crystallization dominated the crystallization process, although surface crystallization occurred simultaneously for glass particles with small size.

References

1. Hench LL, Splinter RJ, Allen WC, Greenlee TK (1971) J Biomed Mater Res 2:117
2. Huang WH, Day DE, Kittiratanapiboon K, Rahaman MN (2006) J Mater Sci Mater Med 17:583
3. Yao AH, Wang DP, Huang WH, Fu Q, Rahaman MN, Day DE (2007) J Am Ceram Soc 90:303
4. Clupper DC, Hench LL (2003) J Non-Crystalline Solids 318:43
5. Kokubo T, Kushitani H, Sakka S, Kitsugi T, Yamamuro T (1990) J Biomed Mater Res 24:721
6. Chen QZ, Thompson ID, Boccaccini AR (2006) Biomaterials 27:2414
7. Yukimitu K, Oliveira RC, Araújo EB, Moraes JCS, Avanci LH (2005) Thermochim Acta 426:157
8. Prasad NS, Varma KBR (2005) J Am Ceram Soc 88:357
9. Matusiata K, Sakka S (1980) J Non-Crystalline Solids 38:741
10. Xu XJ, Ray CS, Day DE (1991) J Am Ceram Soc 74:909

11. Ozawa T (1971) Polymer 12:150
12. Ray CS, Day DE (1996) Thermochim Acta 280/281:163
13. Guedes M, Ferro AC, Ferreira JMF (2001) J Eur Ceram Soc 21:1187
14. Pernice P, Esposito S, Aronne A, Sigaev VN (1999) J Non-Crystalline Solids 258:1
15. Agathopoulos S, Tulyaganov DU, Ventura JMG, Kannan S, Karakassides MA, Ferreira JMF (2006) Biomaterials 27:1832
16. Cheng CT, Lanagan M, Lin JT, Jones B, Pan MJ (2005) J Mater Res 20:438
17. Zhang HY, Mitchell BS (2000) J Mater Res 15:1000
18. Marion NW, Liang W, Reilly GC, Day DE, Rahaman MN, Mao JJ (2005) Mech Adv Mater Struct 12:39
19. Rahaman MN, Liang W, Day DE, Marion NW, Reilly GC, Mao JJ (2005) Ceram Eng Sci Proc 26:3
20. Richard MNC (2000) M.S. Thesis, University of Misssouri-Rolla
21. Fillo OP, LaTorre GP, Hench LL (1996) J Biomed Mater Res 30:509
22. Li P, Yang Q, Zhang F, Kokubo T (1992) J Biomed Mater Res 3:452